



Originally published as:

Kim, H., Shiokawa, K., Park, J., Miyoshi, Y., Miyashita, Y., Stolle, C., Kim, K., Matzka, J., Buchert, S., Fromm, T., Hwang, J. (2020): Ionospheric Plasma Density Oscillation Related to EMIC Pc1 Waves. - Geophysical Research Letters, 47, 15, e2020GL089000.

<https://doi.org/10.1029/2020GL089000>

Geophysical Research Letters

RESEARCH LETTER

10.1029/2020GL089000

Special Section:

Probing the Magnetosphere through Magnetoseismology and Ultra-Low-Frequency Waves

Key Points:

- We report the first observation of ionospheric plasma density oscillation correlated with electromagnetic ion cyclotron (EMIC) Pc1 wave
- Simple MHD theory cannot explain the observed amplitude and phase relationships between the plasma density oscillation and the Pc1 wave
- The EMIC Pc1 wave was also accompanied by localized proton precipitation

Supporting Information:

- Supporting Information S1

Correspondence to:

H. Kim,
kim.hyangpyo@isee.nagoya-u.ac.jp

Citation:










Kim, H., Shiokawa, K., Park, J., Miyoshi, Y., Miyashita, Y., Stolle, C., et al. (2020). Ionospheric plasma density oscillation related to EMIC Pc1 waves. *Geophysical Research Letters*, 47, e2020GL089000. <https://doi.org/10.1029/2020GL089000>

Received 24 MAY 2020

Accepted 8 JUL 2020

Accepted article online 19 JUL 2020

Ionospheric Plasma Density Oscillation Related to EMIC Pc1 Waves

Hyangpyo Kim¹ , Kazuo Shiokawa¹, Jaeheung Park^{2,3} , Yoshizumi Miyoshi¹ , Yukinaga Miyashita² , Claudia Stolle⁴ , Khan-Hyuk Kim⁵ , Jürgen Matzka⁴ , Stephan Buchert⁶ , Tanja Fromm⁷, and Junga Hwang^{2,3} 

¹Institute for Space-Earth Environmental Research, Nagoya University, Nagoya, Japan, ²Korea Astronomy and Space Science Institute, Daejeon, South Korea, ³Korea University of Science and Technology, Daejeon, South Korea, ⁴GFZ German Research Centre for Geosciences, Potsdam, Germany, ⁵School of Space Research, Kyung Hee University, Gyeonggi, South Korea, ⁶Swedish Institute of Space Physics, Uppsala, Sweden, ⁷Alfred-Wegener-Institut für Polar- und Meeresforschung, Bremerhaven, Germany

Abstract We report the first observation of plasma density oscillations coherent with magnetic Pc1 waves. Swarm satellites observed compressional Pc1 wave activity in the 0.5–3 Hz band, which was coherent with in situ plasma density oscillations. Around the Pc1 event location, the Antarctic Neumayer Station III (L ~ 4.2) recorded similar Pc1 events in the horizontal component while NOAA-15 observed isolated proton precipitations at energies above 30 keV. All these observations support that the compressional Pc1 waves at Swarm are oscillations converted from electromagnetic ion cyclotron (EMIC) waves coming from the magnetosphere. The magnetic field and plasma density oscillate in-phase. We compared the amplitudes of density and magnetic field oscillations normalized to background values and found that the density power is much larger than the magnetic field power. This difference cannot be explained by a simple magnetohydrodynamic (MHD) model, although steep horizontal/vertical gradients of background ionospheric density can partly reconcile the discrepancy.

Plain Language Summary Electromagnetic ion cyclotron (EMIC) wave is known to be generated in the inner magnetosphere in the ultralow frequency (ULF) Pc1 range (0.2–5 Hz). The EMIC Pc1 waves propagate as shear Alfvén mode from the magnetospheric source toward the ionosphere. On arriving at ionospheric altitudes, they undergo mode conversion to the compressional Alfvén mode due to the Hall conductivity. According to the ideal magnetohydrodynamics (MHD) theory, the compressional ULF wave can be accompanied by density perturbation of ionospheric plasmas. In this paper, we report the first observation of ionospheric plasma density oscillations driven by EMIC Pc1 waves based on the observation by the Swarm satellites. Simple MHD equations cannot fully explain the amplitude and phase relationship between plasma density and magnetic Pc1 pulsations, while steep horizontal/vertical gradients of background ionospheric plasma density may in part reconcile the discrepancy.

1. Introduction

Electromagnetic ion cyclotron (EMIC) waves are typically generated intermittently in the inner magnetosphere as a result of ion cyclotron instability and are observed in the ultralow frequency (ULF) Pc1 range (0.2–5 Hz). Other origins of EMIC waves in the inner magnetosphere are summarized in Miyoshi et al. (2019). EMIC waves typically propagate along the ambient magnetic field as shear Alfvén mode. Still, when the waves arrive at the highly conductive ionosphere, they undergo mode conversion to the compressional mode (or fast mode), which enables wave ducting along the ionosphere (Fujita & Tamao, 1988; Kim et al., 2020; Yoshikawa, 2002).

According to the ideal magnetohydrodynamic (MHD) wave theory, ULF waves can be accompanied by density perturbation when they propagate in compressional mode. In other words, EMIC waves are not only affected by ionospheric plasma but also actively control it by modulating plasma density. This expectation, however, has not yet been confirmed observationally due to the lack of sufficient in situ data. Until now, only ULF Pc3–Pc5 waves (2–100 mHz) have been reported to accompany pulsations of ionospheric total electron content (TEC) in similar frequency ranges (Belakhovsky et al., 2016; Davies & Hartman, 1976; Okuzawa &

Davies, 1981; Pilipenko, Belakhovsky, Kozlovsky, et al., 2014; Pilipenko, Belakhovsky, Murr, et al., 2014; Vorontsova et al., 2015; Watson et al., 2015, 2016).

By the Swarm satellites launched on 22 November 2013, it has become possible to simultaneously detect both magnetic field and plasma density oscillations up to the Pc1 frequency range. In this paper, we report ionospheric plasma density oscillations accompanied by compressional oscillations associated with EMIC Pc1 waves based on Swarm measurements. Section 2 briefly describes the satellite and the data set used, and observation results are presented in section 3. We discuss our observation results in section 4 in the context of MHD equations. Finally, a summary and conclusions are given in section 5.

2. Data Description

Swarm is a low Earth orbit satellite constellation placed on two different polar orbits. Swarm-A and Swarm-C move side by side at an altitude of ~ 450 km, and Swarm-B flies alone at an altitude of ~ 530 km. The Vector Field Magnetometer (VFM) measures the three-axis magnetic field with a high sampling rate of 50 Hz and a resolution of 0.01 nT. Swarm Langmuir Probe (LP) provides electron density measurements derived from faceplate currents with a 16-Hz sampling rate (Buchert, 2016). Induction magnetometer data from the Neumayer Station III (VNA) in Antarctica are used to identify EMIC Pc1 waves at auroral/subauroral region. The ground station is located at a geographic longitude of 8.3°W , a geographic latitude of 70.7°S , and on a magnetic L shell of 4.2 according to the Altitude Adjusted Corrected Geomagnetic (AACGM) system (Shepherd, 2014). The magnetic field data are provided at 0.05-s resolution.

We generally follow the data processing scheme described by Kim, Hwang, Park, Bortnik, et al. (2018), Kim, Hwang, Park, Miyashita, et al. (2018), and Kim et al. (2020), which are only briefly summarized here. We used a second-order Savitzky-Golay smoothing filter to define the respective backgrounds of both the magnetic field and electron density of Swarm. Local field-aligned coordinates are used to extract transverse (x : toward outer L-shells; y : toward magnetic east) and compressional (z : parallel to the background B field) electromagnetic pulsations. For cross-spectral analysis, we interpolated the 50-Hz magnetic field residual down to 16 Hz, which is the electron density sampling rate. Finally, fast Fourier transform (FFT) with a window size of 512 data points (32 s) is applied to both of the residual data to obtain their spectra. We estimated the spectra every 10 s using a moving window of 32-s length.

3. Observations

Figures 1a–1c show Fourier spectrograms of transverse (δB_x and δB_y) and compressional magnetic field residuals (δB_z) observed by Swarm-A on 4 November 2018. During that time, Swarm-A and Swarm-C traversed the auroral region, and Pc1 waves containing a distinct compressional component were detected by both Swarm-A and Swarm-C (not shown here) from 20:53 to 21:06 UT in the frequency range of 0.5–3 Hz. The strong broadband reddish signals in the transverse components (panels a and b) are caused by field-aligned current-associated magnetic field oscillations, which are generally detected whenever a satellite crosses the auroral zone. Note that Swarm-B at that time was away from the location of the Pc1 event.

Figure 1d shows a Fourier spectrogram of electron density residual (δN_e) superposed with a line plot of electron density as derived from the Swarm LP/faceplate currents. Distinct narrow-band pulsations were nearly simultaneously observed in the frequency band of the enhanced compressional Pc1 wave from 20:56 to 21:02 UT. The intensity of plasma density fluctuations increases when Swarm crosses a sharp density gradient between 20:56 and 20:57 UT. The strong signals below 1 Hz between 20:49 and 20:54 UT are out of our interest because the broadband spectral shapes are totally different from those of the narrow-band Pc1 wave. They rather seem to represent high-latitude irregularities and concomitant magnetic perturbations (e.g., Laundal et al., 2019).

In order to analyze the phase relationship between compressional Pc1 wave and density oscillations, we conducted a cross-spectral analysis of δB_z and δN_e . The original time series of both δB_z and δN_e are in Figures s1c and s1d in the supporting information. Figure 1e shows coherency spectra (γ), which identify the linear correlation between the two signals. If γ is unity, δB_z and δN_e oscillations are completely identical while they are entirely unrelated or incoherent if γ is 0. To concentrate on high-amplitude signals above the background noise level, we exclude signals in which the median-subtracted power spectral densities of δB_z for each

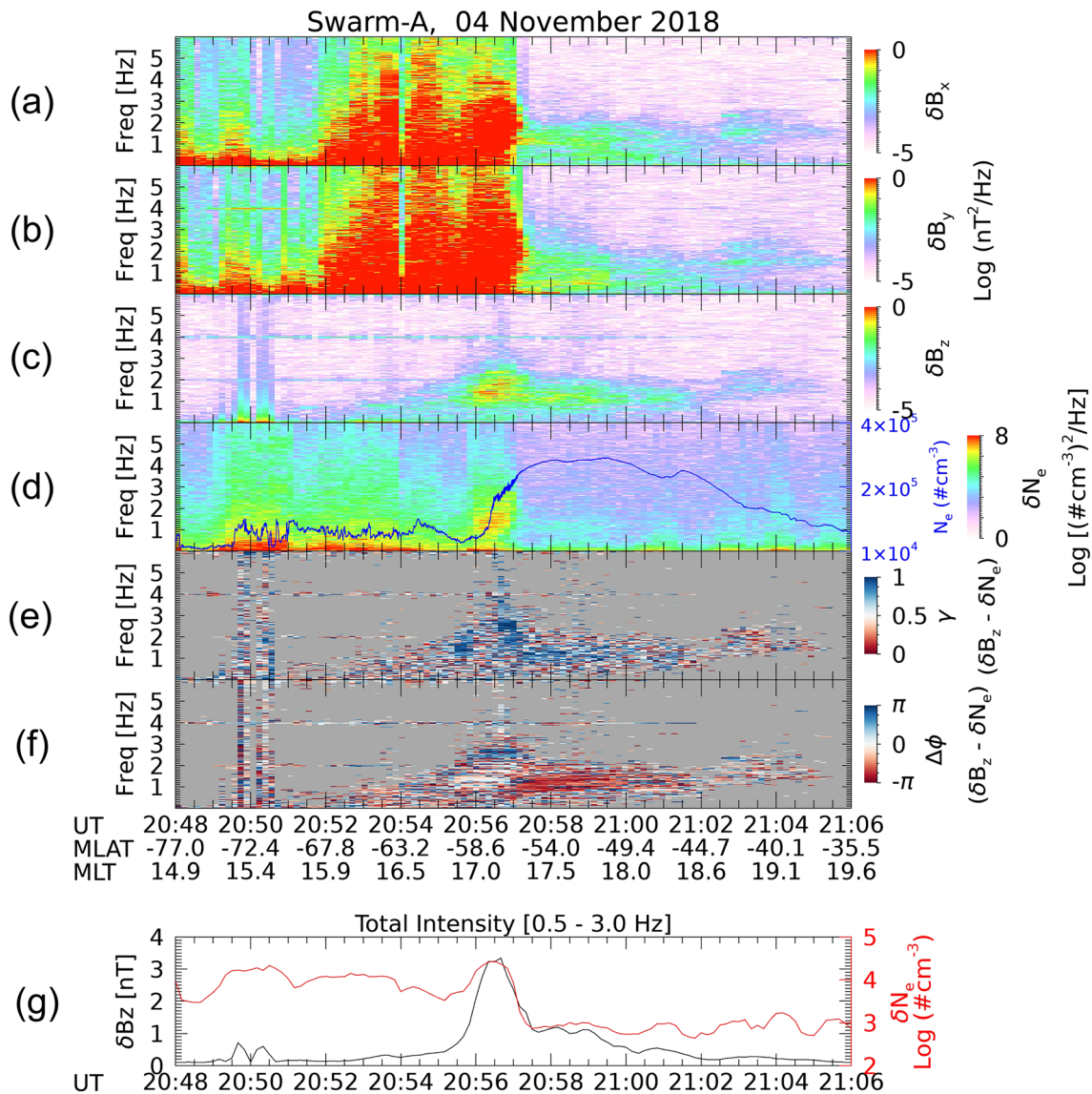


Figure 1. Stacked plot of Swarm-A observations on 4 November 2018. (a, b) Fourier spectrograms of transverse (δB_x and δB_y) and (c) compressional magnetic field residual (δB_z) in local field-aligned coordinates. (d) Fourier spectrogram of electron density residual (δN_e) superposed with original N_e readings (blue line). (e) Coherency spectra between δB_z and δN_e , and (f) phase-difference between δB_z and δN_e . (g) The total sum of FFT wave amplitudes over the frequency bins within 0.5–3.0 Hz for δB_z (black line) and δN_e (red line).

frequency during the plotted interval are less than unity on the logarithmic scale (see Bortnik et al., 2007, for details of the filter): These points are colored in gray. As shown in Figure 1e, γ is high (close to 1: blue color) when the oscillation intensities in both δB_z and δN_e are high.

Next, we calculate the phase difference ($\Delta\phi$) between δB_z and δN_e , and the result is shown in Figure 1f. The $\Delta\phi$ is a difference in phase angle between two signals. If $\Delta\phi$ is 0, two signals are perfectly in-phase (white color in Figure 1f), while two signals become antiphase if $\Delta\phi$ goes to $|\pm\pi|$ (blue and red colors in Figure 1f). During the strong wave activities in both δB_z and δN_e (20:56–20:57 UT), the two parameters are nearly in-phase (white color) in the main frequency band between 0.5 and 2 Hz, while they showed out-of-phase relationship after 20:57 UT when waves were weak (red color). Note that a population of weaker Pc1 pulsations at higher frequencies (>2.5 Hz; 20:56–20:57 UT) exhibits antiphase relationship (blue color). However, the wave amplitudes (Figures 1c and 1d), especially that of plasma density, are not so high for those two antiphase populations. The overall in-phase relationship can also be seen in Figure s1d.

Figure 1g presents the total sum of FFT wave amplitudes over the frequency bins within 0.5–3.0 Hz for compressional Pc1 wave (black line, in nT) and electron density oscillation (red line, in cm^{-3}). The two wave intensities show a similar temporal variation during the event, particularly from 20:56 to 21:02 UT, during which the similar spectral shapes between two signals were already demonstrated in Figures 1c–1f.

4. Discussion

4.1. Did Swarm Observe Actual EMIC Pc1 Waves?

In the previous section, we showed compressional Pc1 waves accompanied by plasma density oscillations from Swarm observations. Their similar spectral shapes and temporal changes of intensity, as well as the high coherency, imply that the Pc1 waves generate the density oscillation as expected from the MHD theory. However, one may also suspect that the plasma irregularities may have driven the compressional magnetic pulsations via a diamagnetic effect (Laundal et al., 2019; Stolle et al., 2006). In this case, there would be no actual electromagnetic wave, but the spatially structured diamagnetic signals can be misinterpreted as Pc1 pulsations by the moving Swarm platform due to the Doppler effect. Hence, we need further pieces of evidence to support that the Pc1 waves observed by Swarm are oscillations generated through mode conversion of transverse EMIC waves originating from the magnetosphere to compressional waves. Below, we investigate conjunction observations from other satellites and ground stations.

As EMIC waves are known to precipitate energetic protons into the atmosphere through resonant wave-particle interactions (Miyoshi et al., 2008; Yahnin & Yahnina, 2007), localized precipitation of proton flux has been conventionally used as evidence for the existence of EMIC waves (e.g., Kim et al., 2016; Yahnin et al., 2016). Besides, ground-based observations of Pc1 pulsations can also support the existence of real EMIC waves. Ground magnetometers, unlike Swarm, are free from the Doppler effect that leads to misinterpreting ionospheric irregularities as electromagnetic waves. During our event, we found two conjunction observations: wave observations by the Antarctic Neumayer station III (VNA) and proton precipitation by the NOAA-15 satellite, respectively.

Figure 2a shows the footprints of Swarm and the NOAA-15 satellite and the location of VNA station ($L \sim 4.2$, 70.7°S , 8.3°W). During this period, Swarm and NOAA-15 flew over the VNA station with only a 2-min time difference. Here we marked a period of intense wave activity at Swarm and a period of proton precipitation at NOAA-15 as thick lines that correspond to blue and red squares in Figures 2b and 2c, respectively.

Figure 2b shows the Fourier spectrogram of δB_z observed by Swarm-A and that of the horizontal magnetic field residual (δH) observed at VNA. VNA observed Pc1 waves similar to the Swarm observations, especially in the main frequency range between 0.5 and 2 Hz even though the intensities are weak. In order to check whether the VNA Pc1 event is above the noise level, we excluded frequency bins for which the daily median-subtracted power spectral densities of δH are less than unity on the logarithmic scale, as was done for Figures 1e and 1f (gray colors). The Pc1 pulsations are still visible in this result (not shown here), which implies that the pulsations at VNA represent geophysical Pc1 waves above the noise level. The absence of high frequencies (>2 Hz) in VNA observations during 20:54–21:02 UT may be because higher-frequency Pc1 waves are generally more difficult to penetrate down to the ground (e.g., Fedorov et al., 2018). Hence, the VNA observations of Pc1 pulsations support that the Pc1 wave observed by Swarm is not a Doppler-shifted ionospheric irregularity, but an actual EMIC wave.

Figure 2c shows proton fluxes observed by the MEPED instrument of the NOAA-15 satellite (Evans & Greer, 2000). The blue lines indicate precipitating protons, and black lines indicate locally trapped (or mirroring) protons along the magnetic field. The isolated proton precipitations in all energy channels were detected from 20:58:20 to 20:59:20 UT. As mentioned in a previous paragraph, the isolated peaks are generally deemed as signatures of EMIC waves. Note that there is a slight time difference of a few minutes between the intense Pc1 wave activity and proton precipitation (blue and red squares). However, the satellite footprints of the two phenomena were very close to each other at these two times, as shown in Figure 2a (thick lines). These observations verify that the Swarm passed over the wave injection region, and observed EMIC waves that propagated from the magnetospheric source region down to the ground.

According to Stolle et al. (2006) and Laundal et al. (2019), diamagnetic effects of ionospheric irregularities generally result in a 180° phase difference between plasma density and compressional magnetic residuals.

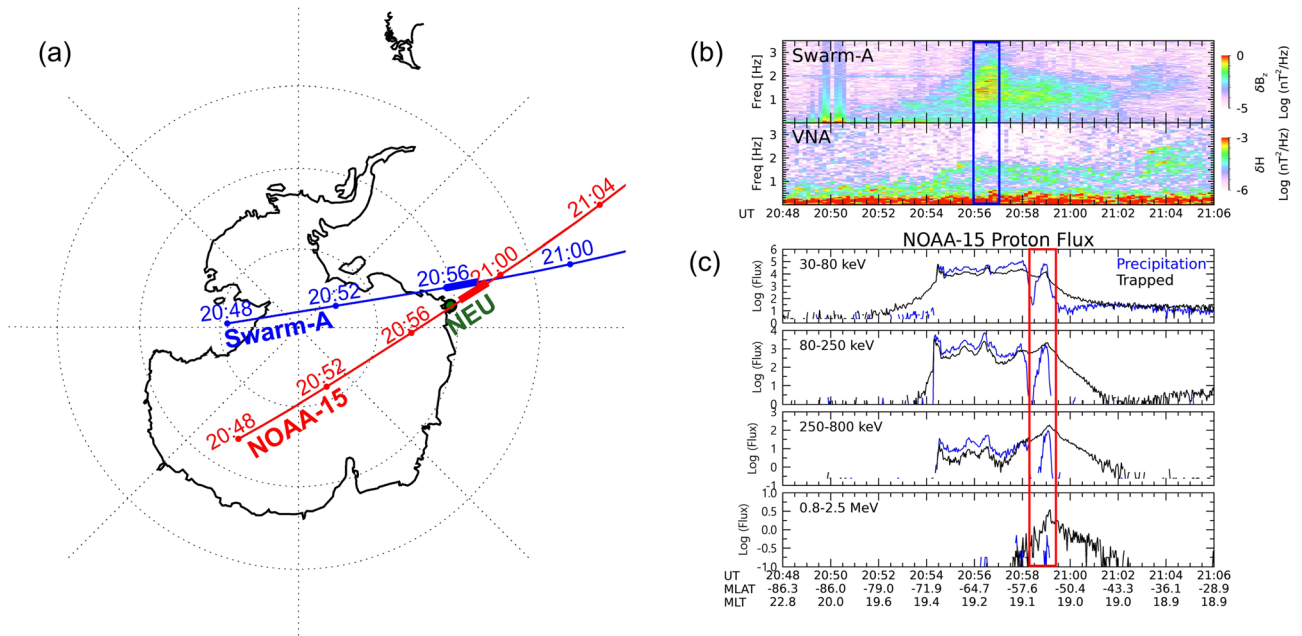


Figure 2. (a) Satellite footprints of Swarm and NOAA-15 satellites, and the location of Antarctic Neumayer Station III (VNA) ($L \sim 4.2$, 70.7°S , 8.3°W). (b) Fourier spectrograms of compressional magnetic field residual (δB_z) observed by Swarm-A and horizontal magnetic field residual (δH) observed by VNA. (c) NOAA-15 proton fluxes. The blue and red squares, respectively, indicate the periods of strong wave activity and proton precipitation, which correspond to the thick lines on the satellite trajectories in (a).

On the other hand, a minority of irregularities with exceptionally high-temperature changes may lead to an in-phase relationship (Rodríguez-Zuluaga et al., 2019). Hence, we cannot entirely discard the possibility that the diamagnetic effect of preexisting plasma irregularities (even without actual Pc1 waves) may have caused the nearly in-phase relationship between plasma density undulations and compressional Pc1 (Figure 1f) on 4 November 2018. Since the powers of δB_z and δN_e are most enhanced at around 2 Hz, we checked 2-Hz spot readings of electron temperature by the LP. But the temperature varied only by about 10% within the interval between 20:56 and 20:57 UT with an average value of 2,450 K.

In addition, we theoretically check whether our event can result from diamagnetic effects of preexisting ionospheric irregularities. We first estimate the necessary temperature variations based on the equation of Laundal et al. (2019, equation 1). The isothermal assumption is removed (e.g., Rodríguez-Zuluaga et al., 2019, equation 4) since a constant temperature cannot explain the observed in-phase relationship in Figure 1f. By assuming the temperatures of electron and ion are the same, the temperature variations required can be expressed as

$$\delta T_e = \frac{\left[-\frac{\delta B_z B_0}{\mu_0} \left(\frac{1}{2k_B} \right) - \delta N_e T_{e0} \right]}{N_{e0} + \delta N_e}, \quad (1)$$

where N_{e0} , B_0 , and T_{e0} on the right-hand side are respective background levels of electron density, magnetic field, and electron temperature, while μ_0 is the vacuum permeability, and k_B is the Boltzmann's constant. δT_e on the left-hand side is the fluctuation level of electron temperature needed to explain the observed compressional Pc1 amplitude. By inputting realistic values ($\delta B_z \sim 3$ nT, $\delta N_e \sim 10^4$ cm^{-3} , and $N_{e0} \sim 10^5$ cm^{-3} as seen in Figure 1; $B_0 \sim 3 \times 10^4$ nT and $T_{e0} \sim 3 \times 10^3$ K observed by Swarm during this event but not shown here), we obtain $\delta T_e > 20,000$ K, almost an order higher than the background value. This is by far too large if we consider previous reports on localized electron temperature changes in the topside ionosphere (e.g., Liang et al., 2017, figure 6a; Oyama et al., 1988, figure 6; Rodríguez-Zuluaga et al., 2019). Hence, it is more plausible to interpret our event as real EMIC Pc1 waves than as the diamagnetic effects of preexisting ionospheric irregularities. Moreover, ionospheric irregularities are generally broad-banded

themselves (Ivarsen et al., 2019, figure 1) or incur broad-band magnetic fluctuations (e.g., Lühr et al., 2014, figure 1; Laundal et al., 2019, figure 3), which is different from narrow-banded Pc1 electromagnetic waves (e.g., Yin et al., 2019, figure 4, and related discussions). Hence, the limited bandwidth of the Pc1 event in Figure 1 suggests that the pulsations are not diamagnetic signatures of ionospheric irregularities.

4.2. Comparison to the Ideal MHD Wave Theory

In this subsection, we compare our observations to the MHD wave theory. We assume that the waves propagate at the Alfvén velocity in cold plasma and ignore plasma-neutral collision effects. Both assumptions are valid in the ionospheric *F* layer around the Swarm altitude and in the Pc1 frequency range. To obtain simple analytic solutions, we further assume homogeneous background magnetic field and horizontal propagation of the wave along the ionospheric duct. We derived the following relationship between density oscillation and compressional ULF Pc1 waves in the ionosphere, details of which are available at Appendix A:

$$\frac{\delta N_e}{N_{e0}} = \frac{\delta B_z}{B_0} \left\{ 1 + \frac{1}{\sin^2 \theta} \left[\frac{1}{kH_x} - \cos \theta \left(\frac{\sin \theta}{kH_z} + \frac{\cos \theta}{kH_x} \right) \right] i \right\}, \quad (2)$$

where k is the wave number and θ is the wave propagation angle relative to the background magnetic field. H_x and H_z are scale lengths of ionospheric plasma density in the horizontal and vertical directions, respectively, and i stands for the imaginary unit. Note that Equation 2 is valid when the wavelength is less than the inhomogeneity scale, that is, $kH_x \gg 1$ and $kH_z \gg 1$. In the homogeneous background plasma (i.e., infinitely large H_x and H_z), the term inside the curly brackets simply becomes unity. In this case, the relative amplitude (i.e., fluctuation amplitude normalized to the background) of plasma density fluctuation is the same as that of the compressional magnetic field, and the phase difference between the two is zero.

On the contrary, Swarm observations showed the amplitude ratio of the electron density ($\frac{\delta N_e}{N_{e0}} \sim \frac{10^4}{10^5}$) is about 1,000 times of $\frac{\delta B_z}{B_0}$ (Figure 1g) and the two parameters oscillate nearly in-phase in the region of a sharp density gradient (20:56–20:57 UT in Figure 1f). According to Equation 2, when H_x and H_z are finite (i.e., nonzero spatial gradient of plasma density), $\frac{\delta N_e}{N_{e0}}$ becomes larger than $\frac{\delta B_z}{B_0}$. This implies that the steep density gradient may play a role in the large differences in the relative pulsation amplitude between the two parameters. However, it is difficult to apply realistic scale lengths (e.g., $H_z \sim 100$ km; Hu et al., 2019) into Equation 2, because k is around 0.01 km^{-1} at Swarm altitudes if we assume the Pc1 wave phase velocity is nearly equal to the Alfvén speed, which is more than a few hundred km/s; see, for example, Pakhotin et al. (2018). The realistic k value ($\approx 0.01 \text{ km}^{-1}$) combined with H_z (≈ 100 km) cannot satisfy the condition, $kH_z \gg 1$. Hence, further theoretical efforts in the future are warranted to solve this problem in a more realistic situation than Equation 2 can.

To compare observations and theory further, we show in Figure 3 another event of plasma density oscillation associated with EMIC Pc1 waves, which occurred on 25 June 2015: refer to Kim et al. (2018) for details of the event. During this period, Swarm observed latitudinally wide ducting of compressional Pc1 waves and corresponding plasma density oscillations (2.8–3.5 Hz) (red square in Figure 3). The relative amplitude of plasma density fluctuation was ~ 100 times that of the compressional magnetic field (Figure 3g). The horizontal scale lengths of ionospheric plasma density are much larger than those in the 4 November 2018 event (i.e., weaker horizontal gradient), which may satisfy $kH_x \gg 1$, to justify the use of Equation 2. However, the observed difference in relative amplitude (~ 100 times) on 25 June 2015 is still too large to be explained by the ideal MHD theory, which can only make the ratio between $\frac{\delta N_e}{N_{e0}}$ and $\frac{\delta B_z}{B_0}$ be of the order of unity when $H_x \gg 1$.

The cross-spectral analyses between δB_z and δN_e revealed a largely out-of-phase relationship (Figures 3f, and see the time series in Figures S2c and S2d) during the whole event period. Though the out-of-phase relationship may not be readily identifiable in the time series in Figure S2d, the high coherence in Figure 3e (blue color) supports the robustness of the 180° phase difference for the ducting event on 25 June 2015. Similarly, during the 4 November 2018 event in Figure 1, Swarm seems to have entered the Pc1 ducting

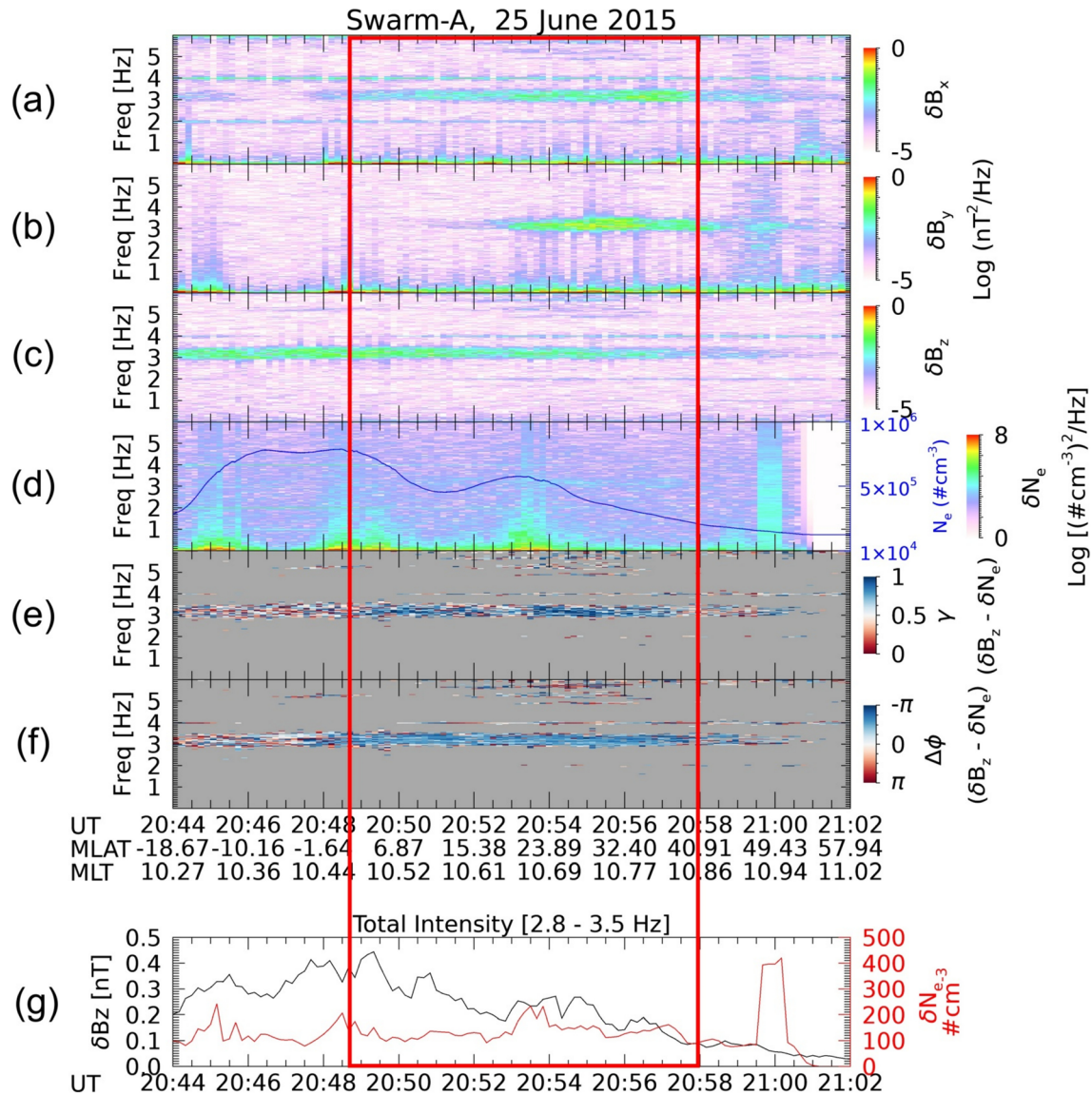


Figure 3. Stacked plot of Swarm-A observations on 25 June 2015 as in Figure 1, but the total sum of FFT wave amplitudes is calculated over the frequency bins within 2.8–3.5 Hz. The red square indicates the period of plasma density oscillation associated with the ducting of EMIC Pc1 wave.

region (i.e., have exited from the wave entry/injection point) after 20:57 UT because (1) the wave intensity abruptly decreased at this point, and (2) NOAA-15 arriving at this region ~2 min after Swarm-A detected no proton precipitation (Figures 2a and 2c). After entering the duct, Swarm continuously observed substantial phase differences, as was observed for the 25 June 2015 event. These results imply that the phase relationship between the compressional Pc1 wave and plasma density oscillation can be different in the wave injection region and the ionospheric duct.

As mentioned before, the Pc1 waves in Figure 1 seem to also include the wave injection region (considering the proton precipitation peaks) where the shear Alfvén wave can be converted to compressional waves. This means that the theory of a purely compressional wave may not be applicable to the present event because shear Alfvén waves should coexist there, albeit masked by strong auroral currents in Figures 1a and 1b. Thus, it is worth theoretically investigating plasma density oscillations associated with more realistic compressional/perpendicular Pc1 waves in future studies.

4.3. Comparison to Previous Studies for Lower-Frequency ULF Waves

In section 3, we reported coherent Pc1 waves in electron density and magnetic field for the first time in the upper ionosphere. As for frequency ranges much lower than the Pc1 (e.g., Pc3–Pc5), on the other hand, there have been several studies on the collocated pulsations of the magnetic field and ground-based TEC. For example, TEC modulation by strong ULF Pc5 waves during the recovery phase of the Halloween storm (31 October 2003) showed that the amplitude ratio of TEC oscillations was 2.5 times that of the geomagnetic pulsations and the average phase difference was $\Delta\phi \sim 100^\circ$ (Pilipenko, Belakhovsky, Kozlovsky, et al., 2014; Pilipenko, Belakhovsky, Murr, et al., 2014), which is different from our Swarm observations. They suggested several mechanisms by which Pc5 waves can modulate TEC, including vertical plasma drift by incident Alfvén wave, ion heating by Pc5 wave electric field, and field-aligned plasma transport by Alfvén waves. For the event studied by Watson et al. (2015), the amplitude of TEC oscillations was 200 times that of geomagnetic pulsations, and they suggested that energetic electron precipitations mainly contribute to the large magnitude of the TEC oscillations. According to a recent study by Kozyreva et al. (2020), localized steep plasma density gradient in the topside ionosphere may be sufficient to produce TEC modulation associated with Pc5 wave. However, direct comparison between those TEC oscillations and Swarm observations is difficult, because TEC is integrated electron density along a satellite-to-receiver raypath, which can mask plasma oscillations that are localized to a limited altitude range. Besides, the amplitude of ULF Pc5 waves (up to a few hundred nT) is much stronger than that of Pc1 waves in the ionosphere (a few nT or smaller) (e.g., Park et al., 2013; Kim et al., 2018).

Among the mechanisms suggested by the studies mentioned above, field-aligned plasma supply/depletion by Alfvén waves seems inapplicable to our Swarm observations. According to Belakhovsky et al. (2016), field-aligned plasma transport induced by Alfvén waves is a dominant modulation mechanism to periodic TEC variations. However, this mechanism mainly works in the lower ionosphere, up to ~ 150 km, which is the *E* layer and lower *F* layer. For example, their Figure 5a does not show a clear modulation of signatures above 300 km. For our Swarm event, the altitude was >450 km, to which this mechanism cannot be applied.

One may argue that electron precipitations induced by EMIC waves might ionize neutral particles to modulate ionospheric plasma density (e.g., Francia et al., 2020). However, in general, the resonant electron energy of EMIC waves is high (e.g., Miyoshi et al., 2008), and such electrons typically cause ionization below ~ 120 km, that is, *D* region and lower thermosphere and mesosphere (Francia et al., 2020; Turunen et al., 2009, Discussion). Similarly, precipitating protons of >30 keV observed in our Pc1 event (Figure 2) are known to impact ionospheric altitudes of about 110 km (Fang et al., 2007), also far below Swarm. It is hard to imagine ionization below 120 km, if any, can strongly affect Swarm altitudes when we consider strong ion-neutral collisions and concomitantly inefficient plasma transport at <120 km altitude. Hence, excessive ionization induced by precipitating energetic particles may not be relevant to the Pc1 events reported here.

5. Summary and Conclusions

Based on the Swarm satellite data, we presented the first observational evidence of ionospheric plasma oscillations related to EMIC Pc1 wave. The Swarm observations are collocated with localized energetic proton precipitation and ground-based Pc1 observations, which support the existence of EMIC waves. Cross-spectral analyses between the plasma density and magnetic field Pc1 waves showed high coherence, but the amplitude ratio and phase change exhibited characteristics deviating from the ideal MHD wave theory: for example, significantly larger amplitudes than predicted were observed in electron density. This difference cannot be explained by a simple MHD model, although a strong gradient of background plasma density may contribute to the discrepancy.

So far, the conventional understanding of the effect of ULF waves on ionospheric density oscillations has been limited to low-frequency (Pc3–Pc5) ranges and ground-based TEC data. Even though our observations showed interesting results, this phenomenon is still a challenge for simple MHD wave equations. Responsible mechanisms for the observations are to be established yet. Further investigations are warranted based on more events and additional data sets.

Appendix A

We derive the relationship between density oscillation and compressional Alfvén waves in the ionosphere based on the MHD equation of cold plasma.

We assume the plasma is at rest; the background magnetic field is within the two-dimensional $\hat{x}\hat{z}$ plane ($\vec{B}_0 = B_0 \cos \theta \hat{x} + B_0 \sin \theta \hat{z}$), where θ is the angle between \vec{B}_0 and \vec{k} ; and the wave propagates along the horizontal \hat{x} direction ($\vec{k} = k\hat{x}$). The linearized continuity equation by describing the properties of the waves can be expressed as

$$\omega \rho_1 - \rho_0 \vec{k} \cdot \vec{v} - i(\rho_0/H_z) \hat{z} \cdot \vec{v} - i(\rho_0/H_x) \hat{x} \cdot \vec{v} = 0, \quad (\text{A.1})$$

where ω is frequency and \vec{k} is the wave number vector. ρ_0 and ρ_1 are, respectively, background and fluctuation terms of plasma mass density (ρ), and v is plasma flow velocity induced by Alfvén waves. The H_z and H_x indicate scale lengths of ionospheric plasma density variations in the vertical and horizontal directions, respectively. By considering the ion-neutral collision frequency (ν_{in}), the linearized momentum equation can be expressed as

$$\frac{\omega^2}{k^2} \vec{v} - v_s^2 \left(v_x + \frac{i}{kH_z} v_z + \frac{i}{kH_x} v_x \right) \hat{x} - \frac{B_0 \cos \theta}{\rho_0 \mu_0} (B_0 \cos \theta \vec{v} - \vec{B}_0 v_x) + \frac{(B_0 \cos \theta (\vec{v} \cdot \vec{B}_0) - v_x B_0^2)}{\rho_0 \mu_0} \hat{x} + i \frac{\omega^2 \nu_{in}}{k^2 \omega} \vec{v} = 0, \quad (\text{A.2})$$

where $v_s = \sqrt{p_0/\rho_0}$ is sound speed derived from adiabatic pressure law and p_0 is plasma pressure. μ_0 is the vacuum permeability. The linearized Faraday's and Ohm's law can be expressed as

$$\omega \vec{B}_1 + (\vec{k} \cdot \vec{B}_0) \vec{v} - (\vec{k} \cdot \vec{v}) \vec{B}_0 = 0, \quad (\text{A.3})$$

where \vec{B}_1 is magnetic perturbation due to Alfvén waves.

By combining the Equations A.1–A.3 for the flow velocity, we can derive the density fluctuation term,

$$\rho_1 = \frac{k}{\omega} \rho_0 v_x + \frac{i}{\omega H_x} \rho_0 v_x + \frac{i}{\omega H_z} \rho_0 v_z. \quad (\text{A.4})$$

The v_x and v_z can be derived from Equations A.2 and A.3 as follows:

$$v_x = \frac{\omega B_1}{k B_0 \sin \theta} \left[1 - \frac{v_A^2 \cos^2 \theta}{\frac{\omega^2}{k^2} + i \frac{\omega^2 \nu_{in}}{k^2 \omega}} \right], \quad (\text{A.5})$$

$$v_z = v_x \frac{v_A^2 \sin \theta \cos \theta}{\left(\frac{\omega^2}{k^2} - v_A^2 \cos^2 \theta + i \frac{\omega^2 \nu_{in}}{k^2 \omega} \right)}, \quad (\text{A.6})$$

where v_A is Alfvén velocity defined as $\sqrt{B_0^2/\rho_0 \mu_0}$. By inputting the v_x and v_z , Equation (A.4) can be written as

$$\frac{\rho_1}{\rho_0} = \frac{\omega B_1}{k B_0 \sin \theta} \left\{ \left[1 - \frac{v_A^2 \cos^2 \theta \left(\frac{\omega^2}{k^2} - i \frac{\omega^2 \nu_{in}}{k^2 \omega} \right)}{\left(\frac{\omega^2}{k^2} \right)^2 + \left(\frac{\omega^2 \nu_{in}}{k^2 \omega} \right)^2} \right] \left[\frac{k}{\omega} + \frac{i}{\omega H_x} - \frac{i}{\omega H_z} \frac{v_A^2 \sin \theta \cos \theta \left(\frac{\omega^2}{k^2} - v_A^2 \cos^2 \theta - i \frac{\omega^2 \nu_{in}}{k^2 \omega} \right)}{\left(\frac{\omega^2}{k^2} - v_A^2 \cos^2 \theta \right)^2 + \left(\frac{\omega^2 \nu_{in}}{k^2 \omega} \right)^2} \right] \right\}. \quad (\text{A.7})$$

By assuming the waves propagate at the Alfvén velocity ($\frac{\omega}{k} = v_A$), and also ignoring the plasma-neutral collision effects ($\nu_{in} = 0$), finally, we can derive the relationship between plasma density oscillation and compressional magnetic field as follows:

$$\frac{\rho_1}{\rho_0} = \frac{\delta B_z}{B_0} \left\{ 1 + \frac{1}{\sin^2 \theta} \left[\frac{1}{kH_x} - \cos \theta \left(\frac{\sin \theta}{kH_z} + \frac{\cos \theta}{kH_x} \right) \right] i \right\}, \quad (\text{A.8})$$

where δB_z is compressional component of Alfvén waves.

Data Availability Statement

The Swarm VFM and electron density data were obtained online (from <http://swarm-diss.eo.esa.int>). The MICA-S induction coil magnetometer data at VNA are provided by KHU (lead institute, Korea), NHU, and NJIT (USA) and AWI and GFZ (Germany) (through http://mir1.unh.edu/ulf_status.html). NOAA-15 proton precipitation data were downloaded online (at <https://satdat.ngdc.noaa.gov>).

Acknowledgments

We would like to thank the Swarm team for making their data available to the public. This work was supported by Grant NRF-2019R1A6A3A03032669, under the National Research Foundation of Korea (NRF). This work was also supported by JSPS KAKENHI (15H05815, 16H06286, 15H05747, 17H00728, 20H01955, and 20H01959). J. P. was supported by the Air Force Office of Scientific Research (AFOSR) Grant FA2386-18-1-0107. The work of K.-H. Kim was supported by the Basic Science Research Program through NRF funded by NRF-2019R1F1A1055444.

References

- Belakhovsky, V., Pilipenko, V., Murr, D., Fedorov, E., & Kozlovsky, A. (2016). Modulation of the ionosphere by Pc5 waves observed simultaneously by GPS/TEC and EISCAT. *Earth, Planets and Space*, *68*, 102. <https://doi.org/10.1186/s40623-016-0480-7>
- Bortnik, J., Cutler, J. W., Dunson, C., & Bleier, T. E. (2007). An automatic wave detection algorithm applied to Pc1 pulsations. *Journal of Geophysical Research*, *112*, A04204. <https://doi.org/10.1029/2006JA011900>
- Buchert, S. (2016). Extended EFI LP data FP release notes, *ESA Technical Note*, <https://earth.esa.int/documents/10174/1514862/Swarm-EFI-Extended-LP-Data-Faceplate>
- Davies, K., & Hartman, G. K. (1976). Short-period fluctuations in total columnar electron content. *Journal of Geophysical Research*, *81*(19), 3431–3434. <https://doi.org/10.1029/JA081i019p03431>
- Evans, D. S., & Greer, M. S. (2000). Polar orbiting environmental satellite space environment monitor: 2. Instrument description and archive data documentation, *Tech. Memo. OAR SEC-93*, NOAA, Boulder, Colo
- Fang, X., Ridley, A. J., Liemohn, M. W., Kozyra, J. U., & Evans, D. S. (2007). Global 30–240 keV proton precipitation in the 17–18 April 2002 geomagnetic storms: 3. Impact on the ionosphere and thermosphere. *Journal of Geophysical Research*, *112*, A07310. <https://doi.org/10.1029/2006JA012144>
- Fedorov, E. N., Pilipenko, V. A., Engebretson, M. J., & Hartinger, M. D. (2018). Transmission of a magnetospheric Pc1 wave beam through the ionosphere to the ground. *Journal of Geophysical Research: Space Physics*, *123*, 3965–3982. <https://doi.org/10.1029/2018JA025338>
- Francia, P., Regi, M., De Lauretis, M., Pezzopane, M., Cesaroni, C., Spogli, L., & Raita, T. (2020). A case study of correspondence between Pc1 activity and ionospheric irregularities at polar latitudes. *Earth, Planets and Space*, *72*, 59 (2020). <https://doi.org/10.1186/s40623-020-01184-4>
- Fujita, S., & Tamao, T. (1988). Duct propagation of hydromagnetic waves in the upper ionosphere. 1. Electromagnetic field distributions in high latitudes associated with localized incidence of a shear Alfvén wave. *Journal of Geophysical Research*, *93*(A12), 14,665–14,673. <https://doi.org/10.1029/JA093iA12p14665>
- Hu, A., Carter, B. A., Currie, J. L., Norman, R., Wu, S., Wang, X., & Zhang, K. (2019). Modeling of topside ionospheric vertical scale height based on ionospheric radio occultation measurements. *Journal of Geophysical Research: Space Physics*, *124*, 4926–4942. <https://doi.org/10.1029/2018JA026280>
- Ivarsen, M. F., Jin, Y., Spicher, A., & Clausen, L. B. N. (2019). Direct evidence for the dissipation of small-scale ionospheric plasma structures by a conductive E region. *Journal of Geophysical Research: Space Physics*, *124*, 2935–2942. <https://doi.org/10.1029/2019JA026500>
- Kim, H., Hwang, J., Park, J., Bortnik, J., & Lee, J. (2018). Global characteristics of electromagnetic ion cyclotron waves deduced from Swarm satellites. *Journal of Geophysical Research: Space Physics*, *123*, 1325–1336. <https://doi.org/10.1002/2017JA024888>
- Kim, H., Hwang, J., Park, J., Miyashita, Y., Shiokawa, K., Mann, I. R., et al. (2018). Large-scale ducting of Pc1 pulsations observed by Swarm satellites and multiple ground networks. *Geophysical Research Letters*, *45*, 12,703–12,712. <https://doi.org/10.1029/2018GL080693>
- Kim, H., Shiokawa, K., Park, J., Miyoshi, Y., Hwang, J., & Kadokura, A. (2020). Modulation of Pc1 wave ducting by equatorial plasma bubble. *Geophysical Research Letters*, *47*, e2020GL088054. <https://doi.org/10.1029/2020GL088054>
- Kim, K.-H., Shiokawa, K., Mann, I. R., Park, J.-S., Kwon, H.-J., Hyun, K., et al. (2016). Longitudinal frequency variation of long-lasting EMIC Pc1-Pc2 waves localized in the inner magnetosphere. *Geophysical Research Letters*, *43*, 1039–1046. <https://doi.org/10.1002/2015GL067536>
- Kozyreva, O. V., Pilipenko, V. A., Bland, E. C., Baddeley, L. J., & Zakharov, V. I. (2020). Periodic modulation of the upper ionosphere by ULF waves as observed simultaneously by SuperDARN radars and GPS/TEC technique. *Journal of Geophysical Research: Space Physics*, *125*, e2020JA028032. <https://doi.org/10.1029/2020JA028032>
- Laundal, K. M., Hatch, S. M., & Moretto, T. (2019). Magnetic effects of plasma pressure gradients in the upper F region. *Geophysical Research Letters*, *46*, 2355–2363. <https://doi.org/10.1029/2019GL081980>
- Liang, J., Yang, B., Donovan, E., Burchill, J., & Knudsen, D. (2017). Ionospheric electron heating associated with pulsating auroras: A Swarm survey and model simulation. *Journal of Geophysical Research: Space Physics*, *122*, 8781–8807. <https://doi.org/10.1002/2017JA024127>
- Lühr, H., Park, J., Xiong, C., & Rauberg, J. (2014). Alfvén wave characteristics of equatorial plasma irregularities in the ionosphere derived from CHAMP observations. *Frontiers in Physics*, *2*, 47. <https://doi.org/10.3389/fphy.2014.00047>

- Miyoshi, Y., Matsuda, S., Kurita, S., Nomura, K., Keika, K., Shoji, M., et al. (2019). EMIC waves converted from equatorial noise due to M/Q=2 ions in the plasmapshe: Observations from Van Allen Probes and Arase. *Geophysical Research Letters*, *46*, 5662–5669. <https://doi.org/10.1029/2019GL083024>
- Miyoshi, Y., Sakaguchi, K., Shiokawa, K., Evans, D., Albert, J., Connors, M., & Jordanova, V. (2008). Precipitation of radiation belt electrons by EMIC waves, observed from ground and space. *Geophysical Research Letters*, *35*, L23101. <https://doi.org/10.1029/2008GL035727>
- Okuzawa, T., & Davies, K. (1981). Pulsations in the total columnar electron content. *Journal of Geophysical Research*, *86*(A3), 1355–1363. <https://doi.org/10.1029/JA086iA03p01355>
- Oyama, K. I., Schlegel, K., & Watanabe, S. (1988). Temperature structure of plasma bubbles in the low latitude ionosphere around 600 km altitude. *Planetary and Space Science*, *36*(6), 553–567. [https://doi.org/10.1016/0032-0633\(88\)90025-6](https://doi.org/10.1016/0032-0633(88)90025-6)
- Pakhotin, I. P., Mann, I. R., Lysak, R. L., Knudsen, D. J., Gjerloev, J. W., Rae, I. J., et al. (2018). Diagnosing the role of Alfvén waves in magnetosphere-ionosphere coupling: Swarm observations of large amplitude nonstationary magnetic perturbations during an interval of northward IMF. *Journal of Geophysical Research: Space Physics*, *123*, 326–340. <https://doi.org/10.1002/2017JA024713>
- Park, J., Lühr, H., & Rauberg, J. (2013). Global characteristics of Pc1 magnetic pulsations during solar cycle 23 deduced from CHAMP data. *Annales de Geophysique*, *31*(9), 1507–1520. <https://doi.org/10.5194/angeo-31-1507-2013>
- Pilipenko, V., Belakhovsky, V., Kozlovsky, A., Fedorov, E., & Kauristie, K. (2014). ULF wave modulation of the ionospheric parameters: Radar and magnetometer observations. *Journal of Atmospheric and Solar-Terrestrial Physics*, *108*, 68–76. <https://doi.org/10.1016/j.jastp.2013.12.015>
- Pilipenko, V., Belakhovsky, V., Murr, D., Fedorov, E., & Engebretson, M. (2014). Modulation of total electron content by ULF Pc5 waves. *Journal of Geophysical Research: Space Physics*, *119*, 4358–4369. <https://doi.org/10.1002/2013JA019594>
- Rodríguez-Zuluaga, J., Stolle, C., Yamazaki, Y., Lühr, H., Park, J., Scherliess, L., & Chau, J. L. (2019). On the balance between plasma and magnetic pressure across equatorial plasma depletions. *Journal of Geophysical Research: Space Physics*, *124*, 5936–5944. <https://doi.org/10.1029/2019JA026700>
- Shepherd, S. G. (2014). Altitude-adjusted corrected geomagnetic coordinates: Definition and functional approximations. *Journal of Geophysical Research: Space Physics*, *119*, 7501–7521. <https://doi.org/10.1002/2014JA020264>
- Stolle, C., Lühr, H., Rother, M., & Balasis, G. (2006). Magnetic signatures of equatorial spread F as observed by the CHAMP satellite. *Journal of Geophysical Research*, *111*, A02304. <https://doi.org/10.1029/2005JA011184>
- Turunen, E., Verronen, P. T., Seppälä, A., Rodger, C. J., Clilverd, M. A., Tamminen, J., et al. (2009). Impact of different energies of precipitating particles on NOx generation in the middle and upper atmosphere during geomagnetic storms. *Journal of Atmospheric and Solar-Terrestrial Physics*, *71*(10-11), 1176–1189. <https://doi.org/10.1016/j.jastp.2008.07.005>
- Vorontsova, E., Pilipenko, V., Fedorov, E., Sinha, A. K., & Vichare, G. (2015). Modulation of total electron content by global Pc5 waves at low latitudes. *Advances in Space Research*, *57*, 309–319. <https://doi.org/10.1016/j.asr.2015.10.041>
- Watson, C., Jayachandran, P. T., Singer, H. J., Redmon, R. J., & Danskin, D. (2015). Large-amplitude GPS TEC variations associated with Pc5–6 magnetic field variations observed on the ground and at geosynchronous orbit. *Journal of Geophysical Research: Space Physics*, *120*, 7798–7821. <https://doi.org/10.1002/2015JA021517>
- Watson, C., Jayachandran, P. T., Singer, H. J., Redmon, R. J., & Danskin, D. (2016). GPS TEC response to Pc4 “giant pulsations”. *Journal of Geophysical Research: Space Physics*, *121*, 1722–1735. <https://doi.org/10.1002/2015JA022253>
- Yahnin, A. G., & Yahnina, T. A. (2007). Energetic proton precipitation related to ion-cyclotron waves. *Journal of Atmospheric and Solar-Terrestrial Physics*, *69*, 1690–1706. <https://doi.org/10.1016/j.jastp.2007.02.010>
- Yahnin, A. G., Yahnina, T. A., Semenova, N. V., Gvozdevsky, B. B., & Pashin, A. B. (2016). Relativistic electron precipitation as seen by NOAA POES. *Journal of Geophysical Research: Space Physics*, *121*, 8286–8299. <https://doi.org/10.1002/2016JA022765>
- Yin, F., Lühr, H., Park, J., & Wang, L. (2019). Comprehensive analysis of the magnetic signatures of small-scale traveling ionospheric disturbances, as observed by Swarm. *Journal of Geophysical Research: Space Physics*, *124*, 10,794–10,815. <https://doi.org/10.1029/2019JA027523>
- Yoshikawa, A. (2002). Excitation of a Hall-current generator by field-aligned current closure, via an ionospheric, divergent Hall-current, during the transient phase of magnetosphere-ionosphere coupling. *Journal of Geophysical Research*, *107*(A12), 1145. <https://doi.org/10.1029/2001JA009170>